RAA 2016 Vol. **16** No. **1**, 14 (12pp) doi: 10.1088/1674–4527/16/1/014
http://www.raa-journal.org *http://iopscience.iop.org/raa*

Research in Astronomy and Astrophysics

Geoeffectiveness of the coronal mass ejections associated with solar proton events

Gui-Ming Le[1,3], Chuan Li[2], Yu-Hua Tang[2], Liu-Guan Ding[4], Zhi-Qiang Yin[3], Yu-Lin Chen[4], Yang-Ping Lu[1,4], Min-Hao Chen[1,4] and Zhong-Yi Li[1,4]

[1] Key Laboratory of Space Weather, National Center for Space Weather, China Meteorological Administration, Beijing 100081, China; *legm@cma.gov.cn*
[2] School of Astronomy and Space Science, Nanjing University, Xianlin Campus, Nanjing 210046, China
[3] National Astronomical Observatories, Chinese Academy of Sciences, Beijing 100012, China
[4] School of Mathematics and Statistics, Nanjing University of Information Science and Technology, Nanjing 210044, China

Received 2015 May 2; accepted 2015 July 14

Abstract The intensity-time profiles of solar proton events (SPEs) are grouped into three types in the present study. The Type-I means that the intensity-time profile of an SPE has one peak, which occurs shortly after the associated solar flare and coronal mass ejection (CME). The Type-II means that the SPE profile has two peaks: the first peak occurs shortly after the solar eruption, the second peak occurs at the time when the CME-driven shock reaches the Earth, and the intensity of the second peak is lower than the first one. If the intensity of the second peak is higher than the first one, or the SPE intensity increases continuously until the CME-driven shock reaches the Earth, this kind of intensity-time profile is defined as Type-III. It is found that most CMEs associated with Type-I SPEs have no geoeffectiveness and only a small part of CMEs associated with Type-I SPEs can produce minor (–50 nT $\leq$ Dst $\leq$ –30 nT) or moderate geomagnetic storms (–100 nT$\leq$ Dst $\leq$ –50 nT), but never an intense geomagnetic storm (–200 nT $\leq$ Dst < -100 nT). However, most of the CMEs associated with Type-II and Type-III SPEs can produce intense or great geomagnetic storms (Dst ≤ -200 nT). The solar wind structures responsible for the geomagnetic storms associated with SPEs with different intensity-time profiles have also been investigated and discussed.

Key words: Sun: coronal mass ejections (CMEs) — Sun: particle emission — Sun: solar-terrestrial relations

1 INTRODUCTION

A solar proton event (SPE) is defined as a solar energetic particle (SEP) event with a peak flux $\geq$10 pfu (particle flux unit, particle $\mathrm{cm}^{-2}\ \mathrm{sr}^{-1}\ \mathrm{s}^{-1}$) in the $E\ \geq$10 MeV channel measured by the *GOES* spacecraft during an SEP event. There are traditionally two types of SEP events, impulsive and gradual. An impulsive SEP event is usually associated with an impulsive solar flare, while a gradual SEP event is always associated with both a solar flare and a coronal mass ejection (CME). The SEPs may only be accelerated by CME-driven shocks or by both CME-driven shocks and the associated flares at the early phase of SEP events (Cane et al. 2003, 2006; Gopalswamy et al. 2002, 2004, 2007; Kahler 2001, 2005; Kahler & Vourlidas 2005; Kallenrode 2003; Li & Zank 2005; Le et al. 2006, 2014; Miroshnichenko 2001; Miroshnichenko et al. 2005; Miroshnichenko & Perez-Peraza 2008; Pérez-Peraza et al. 2009; Qin et al. 2006, 2013; Reames 1999; Simnett 2006; Tylka et al. 2005; Trottet et al. 2015; Zank et al. 2007). After the CME enters the interplanetary medium (the so-called ICME), its driven shock becomes the sole accelerator of the SEPs.

When the shock driven by the associated ICME is approaching an in situ spacecraft, the SEP flux may be enhanced due to the shock acceleration, suggesting that the shock or both the shock and the ICME may pass the spacecraft. Therefore, the properties of the variation of the SEP flux can be used to predict the geoeffectiveness of the CMEs associated with SEP events observed by *GOES* or other spacecraft located at L1 (Smith et al. 2004; Smith & Murtagh 2009; Valtonen et al. 2005).

According to the coronagraph observations from *SOHO*/LASCO (Brueckner et al. 1995), Moon et al. (2005) proposed a geoeffectiveness parameter for CMEs defined by the ratio of the shortest to the longest distances of the CME front measured from the solar center, which can be used to predict the geoffectiveness of the associated CMEs (Kim et al. 2008, 2010). After 2006, CME observations from multiple vantage points became available due to the *STEREO* mission. Using remote sensing and in situ measurements of CMEs, the propagation of the CMEs from the

Sun to 1 AU can be tracked and the geoeffectiveness of the CMEs can be predicted (Liu et al. 2010a,b).

Considering the fact that *SOHO* may cease to operate in the near future after being in service for about 20 years, and that *STEREO* A and B are continuously changing their positions, *GOES* is an important source to provide routine observations of SEP events in geostationary orbit. When an SPE occurs, will the CME associated with the SPE reach the Earth and cause a geomagnetic storm? Is it possible to predict geomagnetic storms by only using the SEP data observed by *GOES*? This is the motivation of the paper. We focus on the geoeffectiveness of CMEs accompanied by SPEs with different intensity-time profiles that occurred during solar cycle 23. The solar wind structures responsible for the main phase of geomagnetic storms associated with SPEs with different intensity-time profiles will also be investigated.

This paper is organized as follows: Section 2 describes the data sources and the definition of three types of SPEs applied in this study. In Section 3, we describe geomagnetic storms accompanied by SPEs with different intensity-time profiles and the interplanetary (IP) sources responsible for the main phases of geomagnetic storms. Sections 4 and 5 are devoted to discussion and conclusions, respectively.

2 DATA AND DEFINITIONS

GOES observes both the $E \geq$10 MeV proton data and solar soft X-ray flux data in the 1–8 Å channel. The *ACE* 64-s data are applied to analyze the properties of solar wind plasma. Geomagnetic storms are the result of interactions between solar wind plasma and the magnetosphere. The SYM-H index can be regarded as an approximation of the Dst index with a 1-min resolution (Wanliss & Showalter 2006), and has been widely used to define a geomagnetic storm (Hutchinson et al. 2011 and reference therein). A sudden storm commencement (SSC) is caused by the global compression of the magnetosphere as the result of IP disturbances, such as IP shocks and dynamic pressure pulses (Wilken et al. 1982; Tsurutani et al. 1995; Takeuchi et al. 2002; Bisi et al. 2010). When a strong IP shock reaches the Earth, a sudden enhancement of SEP flux can be observed by *GOES*, along with an abruptly enhanced SYM-H index. This property can help us to judge whether an SEP event is accompanied by a geomagnetic storm. In this study, both Dst and SYM-H index are employed as geomagnetic storm indexes. According to the Dst criteria used to define a geomagnetic storm, a geomagnetic storm with –30 nT $\leq$ Dst $<$ –50 nT is recognized as a minor storm, –100 nT$\leq$ Dst $<$ –50 nT as a moderate storm, –200 nT $\leq$ Dst $<$ –100 nT as an intense storm, and Dst $\leq$ –200 nT as a great storm. The projected speed of a CME can be directly obtained from the website: *http://cdaw.gsfc.nasa.gov/CME_list/*, while the solar wind data observed by the spacecraft *ACE* are available from the website: *http://www.srl.caltech.edu/ACE/ASC/*.

Cane et al. (2006) reported three different intensity-time profiles of SEP events. A Type-P profile shows a prompt onset followed by a slow decay, while a Type-S profile peaks at the time that the IP shock arrives. A type-O profile exhibits a prompt onset and an elevated intensity until the shock passes. The aim of their paper is to investigate the roles of flares and shocks in determining SEP element abundances. The intensity-time profiles of SPEs in the current paper are categorized in a somewhat different manner and our purpose is also different from that of Cane et al. (2006). For the SPEs with source locations distributed in the far eastern hemisphere, the intensity of SPE usually increases gradually and peaks days after the eruption of the associated CME, sometimes after the shock has passed (Cane et al. 1988). Such intensity-time profiles are not examined in this paper. Here we categorize the intensity-time profiles of SPEs into three types. The Type-I profile of SPEs features only one peak shortly after an eruption of the associated solar flares and CMEs, followed by decreased particle intensity. SPEs would have their first peak shortly after the eruption of the concurrent solar flares and CMEs. When approaching the magnetosphere, the ICME-driven shock would lead to enhanced particle intensity and a second peak in the SEP intensity-time profile. In case there are two peaks, the intensity-time profile is defined as Type-II or Type-III if the second peak is lower or higher than the first one, respectively. But in the cases without a second peak, if the SPE intensity increases in a sustained manner until the arrival of the IP shock, the intensity-time profile is also defined as Type-III.

3 GEOEFFECTIVENESS OF CMES ACCOMPANIED BY SPES WITH DIFFERENT INTENSITY-TIME PROFILES

For each type of intensity-time profile for SPEs, we use two typical cases to show the geoeffectiveness of CMEs associated with the SPEs. The IP sources responsible for the geomagnetic storms associated with SPEs will also be investigated. The geomagnetic activities associated with each type of profile for the SPEs that occurred during solar cycle 23 will be investigated and presented in a table.

3.1 Geoeffectiveness of CMEs Associated with Type-I SPEs

According to its definition, a Type-I SPE only has one peak, which appears shortly after the eruption of the associated flare and the CME, and is followed by decreased particle intensity. This indicates that the IP shock finally does not reach the magnetosphere (case 1) or the IP shock is too weak to accelerate the SEPs with energy exceeding 10 MeV when it passes the Earth (case 2).

3.1.1 Case 1

An X2.7 solar flare occurred at 08:09 UT, 1998 May 6 in Active Region (AR) 8210 (S12W65), accompanied

by a CME with an initial speed of 1099 km s^{-1}. After the eruption of the flare and the CME, the *GOES* spacecraft observed an SPE shown in the second panel from the top in Figure 1. The flux of $E \geq 10$ MeV protons peaked at 09:45 UT, 1998 May 6, and then declined. Presumably, when the ICME-driven shock reached the magnetosphere, the SEP flux would display a sudden enhancement. However, there was no suddenly boosted particle flux after the climax of the first peak. We can see from the solar wind data shown in Figure 1 that the *ACE* spacecraft did not observe an IP shock or an ICME during 1998 May 7–8. This suggests that the ICME-driven shock and the ICME itself did not reach the magnetosphere. Richardson & Cane (2010) reported that the *ACE* spacecraft did not see any ICME during 1998 May 7–9, confirming the fact that the CME and the CME-driven shock associated with the SPE that occurred on 1998 May 6 finally failed to reach the magnetosphere.

3.1.2 Case 2

An M1.5 flare occurred at 16:03 UT, 2001 January 28 in AR 9313 (S04W59), and was associated with a full halo CME with a linear speed of 916 km s^{-1}. The integrated intensity of >10 MeV protons reached their peak at 06:55 UT, January 29, and then declined. The solar flare, with an integrated intensity of >10 MeV protons, Dst index, and solar wind parameters during the period of 2001 January 28 - February 1 are presented in Figure 2. One can see in Figure 2 that the IP shock was detected by *ACE* at 07:22 UT, 2001 January 31. The shock, illustrated by the dashed vertical line in Figure 2, was driven by the related ICME. However, it can be easily judged from the solar wind data shown in Figure 2 that the ICME was not detected by the spacecraft *ACE*, suggesting that only the ICME-driven shock passed the Earth.

3.1.3 Statistical results

Table 1 lists 54 SPEs with Type-I profile that occurred during solar cycle 23. In the table, SPEs are numbered in column (1), date of the events in column (2), the solar soft X-ray peak time in column (3), the location of ARs in column (4), the NOAA number of the AR in column (5), the solar soft X-ray flare classes in column (6), the linear speed of the CME in column (7), the angular width (AW) of the CME in column (8), the peak intensities of the SPEs in column (9), and the geomagnetic activity intensity expressed by the minimum Dst value in the last column. In the last column, we use Dst value 0 to indicate that the SPE was not accompanied by a geomagnetic storm.

It can be seen from Table 1 that the 42 IP shocks associated with SPEs did not pass the Earth (shown in case 1). Only 13 IP shocks associated with the SPEs were observed by the *ACE* spacecraft, but the corresponding ICMEs associated with the 13 shocks were not observed by *ACE* (shown in case 2). However, the *ACE* spacecraft has never observed an ICME associated with Type-I SPEs.

3.2 Geoeffectiveness of CMEs Associated with Type-II SPEs

This kind of SPE has two flux peaks with the second peak lower than the first one. To investigate the geoeffectiveness of SPEs with a Type-II profile, we give two typical cases: Case 1 presents an example that the solar wind structure responsible for the geomagnetic storm associated with an SPE is a shock sheath. Case 2 shows an example that the solar wind structure responsible for the geomagnetic storm associated with an SPE is a magnetic cloud (MC).

3.2.1 Case 1

On 1998 May 2, AR 8210, located at S15W15, produced an X1.1 flare at 13:42 UT. The flare, identified as class X1.1, was accompanied by a halo CME. Following the X1.1 flare and the halo CME with an initial speed of 938 km s^{-1}, the flux of $E > 10$ MeV protons increased and peaked at 16:50 UT, 1998 May 2 (as shown by the first dashed vertical line in Fig. 3). The CME-driven shock reached the L1 point at 03:00 UT, 1998 May 4, and caused an SSC. As a result, the flux of $E > 10$ MeV protons suddenly became enhanced and reached its second peak (the second dashed vertical line in Fig. 3). Figure 3 displays the 1–8 Å flare X-ray flux, the integrated intensity of $E > 10$ MeV protons, SYM-H index, and the solar wind parameters in the period of 1998 May 2–4. The first proton flux peak occurred shortly after the X1.1 flare, and the second one appeared when the IP shock reached the magnetosphere. The start time of the ICME is shown by the solid vertical line in Figure 3. A great geomagnetic storm (Dst = –205 nT) occurred after the shock reached the magnetosphere. Evidently, the great geomagnetic storm was only caused by the shock sheath, while the ICME made no contribution to the main phase of the great geomagnetic storm.

3.2.2 Case 2

An X3.4 solar flare appeared at 02:40 UT, 2006 December 13, in AR 10930 that was located at S06W24, and was accompanied by a full halo CME with an initial speed of 1774 km s^{-1}. The CME was caught by *SOHO*/LASCO C2 at 02:54 UT, 2006 December 13. The SPE intensity was enhanced after the eruption of the flare and the CME. One can see from the second panel from the top in Figure 4 that the SPE intensity reached its first peak (698 pfu) at 09:25 UT, December 13. The SPE intensity displayed its second peak when the IP shock reached the magnetosphere at 14:14 UT, December 14.

In Figure 4, the first and second dashed vertical lines indicate the first SPE peak and second SPE peak respectively. Figure 4 also displays the solar wind plasma parameters observed by the *ACE* spacecraft. The solid vertical line in Figure 4 indicates the start time of the ICME. It can be seen from Figure 4 that *ACE* detected an IP shock, a sheath and an MC during the period of 2006 December 14–15. An intense geomagnetic storm (Dst = –144 nT)

Table 1 Geoeffectiveness of CMEs Associated with Type-I SPEs during Solar Cycle 23

Event	Solar X-ray flare					CME		>10 MeV	Dst
No.	Date yyyy/mm/dd	Time hh:mm	Location	AR	X-ray peak	Vel. (km s^{-1})	AW (°)	Peak flux (pfu)	(nT)
1	1998/04/20	10:00	S43W90	8194	M1.4	1863	>243	1700	–69
2	1998/05/06	08:00	S11W65	8210	X2.7	1099	190	210	0
3	1998/09/30	13:20	N23W81	8340	M2	DG	DG	1200	–56
4	1998/11/05	19:55	N26W18	8375	M8.4	1118	360	11	0
5	1998/11/14	05:18	N28W90	NA	C1	NA	NA	310	0
6	1999/04/24	13:00	NA	NA	NA	1495	360	32	0
7	1999/06/01	19:30	S15E08	NA	C1.2	1772	360	48	0
8	1999/06/04	07:03	N17W69	8552	M3.9	2230	150	64	0
9	2000/02/18	09:25	S16W87	NA	C1.1	890	118	13	0
10	2000/06/10	17:02	N22W38	9026	M5.2	1108	360	46	0
11	2000/07/22	11:34	N14W56	9085	M3.7	1230	>229	17	0
12	2000/07/27	11:30	N14W75	NA	M1.2	NA	NA	18	0
13	2000/09/12	12:13	S17W09	NA	M1.0	1550	360	320	–39
14	2000/10/16	07:28	N04W90	9193	M2.5	1330	360	15	0
15	2000/10/25	11:25	N00W95	9199	C4.0	NA	NA	15	0
16	2001/01/28	16:00	S04W59	9313	M1.5	651	261	49	–45
17	2001/04/02	21:51	N18W82	9393	X20.0	2505	244	1110	–50
18	2001/04/12	10:28	S19W42	9415	X2.0	1184	360	50	0
19	2001/04/18	02:14	S20W120	9415	C2	NA	NA	321	0
20	2001/05/07	08:55	NA	NA	NA	604	233	30	0
21	2001/06/15	15:20	NA	NA	NA	1701	360	26	0
22	2001/08/09	11:22	S17E19	NA	C3.7	479	175	17	0
23	2001/08/15	23:55	NA	NA	NA	1575	360	493	0
24	2001/09/15	11:28	S21W49	9608	M1.5	195	44	11	0
25	2001/10/01	05:15	S22W91	9628	M9.1	1405	360	2360	0
26	2001/10/22	17:59	S18E16	9672	X1	618	106	24	–40
27	2001/12/26	05:40	N08W54	9742	M7.1	1446	>212	779	–58
28	2001/12/28	20:45	S26E90	9756	X3.4	2216	360	108	0
29	2002/01/14	06:27	S28W83	9772	M4.4	1492	360	15	0
30	2002/02/20	06:12	N12W72	9825	M5	952	360	13	0
31	2002/03/18	02:31	S09W46	NA	M1.0	989	360	53	0
32	2002/03/22	11:14	NA	9866	M1.6	1750	360	16	0
33	2002/04/21	01:51	S14W84	9906	X1	749	69	68	0
34	2002/07/07	11:43	S19W90	10017	M1.0	638	30	22	0
35	2002/08/14	02:12	N09W54	10061	M2.3	1309	133	26	–31
36	2002/08/22	01:57	S07W62	10069	M5.4	998	360	36	0
37	2002/08/24	01:12	S08W81	10069	X3.1	1913	360	317	–38
38	2002/11/09	13:23	S12W29	10180	M4.6	1838	360	404	0
39	2003/05/31	02:24	S07W65	10365	M9.3	1835	360	27	0
40	2003/01/17	22:55	S08E61	10386	M6	1813	360	24	0
41	2003/10/26	18:19	N02W38	10484	X1.3	1537	>171	466	–32
42	2003/11/04	19:29	S19W83	10486	X28	2657	360	100	0
43	2003/12/02	09:48	S13W65	10508	C7.2	1393	>150	86	–55
44	2004/04/11	04:19	S14W47	10588	C9.6	1645	314	35	0
45	2004/09/12	00:56	N04E42	10672	M4.8	1328	360	273	–50
46	2004/09/19	17:12	N03W58	10672	M1.9	NA	NA	57	0
47	2004/11/01	06:50	N12W49	10691	M1.1	925	146	63	0
48	2004/11/10	02:13	N09W49	10696	X2.5	3387	360	300	–33
49	2005/01/17	09:52	N15W25	10720	X3.8	2094	360	4000	0
50	2005/06/16	20:22	N09W87	10775	M4.0	187	44	44	0
51	2005/07/13	14:49	N10W80	10786	M5.0	1423	360	134	0
52	2005/07/27	05:02	N11E90	10792	M3	1787	360	41	0
53	2006/12/06	18:47	S06E63	10930	X6.5	NA	NA	1980	0
54	2006/12/14	22:15	S06W46	10930	X1.5	1042	360	214	0

Notes: NA indicates no data are available; DG: data gap.

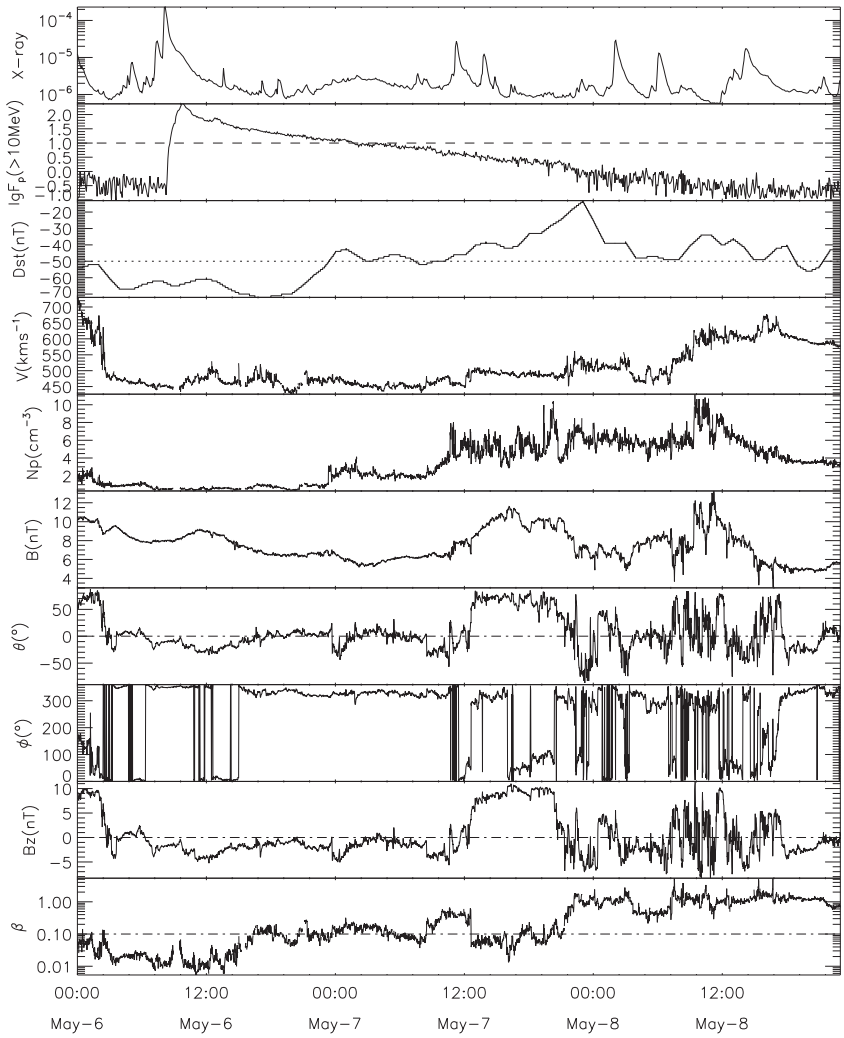

Fig. 1 The solar flare, the flux of $E > 10$ MeV protons, geomagnetic activity and the parameters of solar wind plasma during 1998 May 6–8. From top to bottom: the soft X-ray flux, the flux of >10 MeV protons, Dst index, solar wind speed, proton density, IMF (B), elevation θ, azimuth ϕ, IMF z-component and plasma β.

occurred when the MC reached the magnetosphere. Both the sheath and MC made a contribution to the main phase of the intense geomagnetic storm. However, we can easily judge from Figure 4 that the storm's main phase was almost completely caused by the MC.

3.2.3 Statistical results

Fifteen SPEs with a Type-II profile that occurred during solar cycle 23 and the associated storms are listed in Table 2. In the table, SPEs are numbered in column (1), date of the event in column (2), the solar soft X-ray peak time in column (3), the location of the AR in column (4), the NOAA number of the AR in column (5), the solar soft X-ray flare intensity in column (6), the CME projected speed in column (7), the angular width of the CME in column (8), the peak intensity of the SPE in column (9), the Dst index in column (10), and the interplanetary source (IPS) in the last column. All SPEs listed in Table 2 were accompanied by geomagnetic storms, with four storms being moderate, and the remaining 11 storms being major storms (Dst$\leq$–100 nT). Both the ICMEs and the ICME-driven shocks associated with the SPEs classified as Type-II passed the Earth. We can see from Table 2 that only the geomagnetic storm that occurred on 2006 December 13 was caused by an MC, while the other storms were caused by shock sheaths.

3.3 Geoeffectiveness of CMEs Associated with Type-III SPEs

We give two examples to show what kind of geomagnetic storms will be associated with SPEs with a type-III profile and what kind of solar wind structures will be responsible for the main phases of the storms. Case 1 is an example that shows the SPE intensity increased rapidly and then increased slowly in a sustained manner. Case 2 is an exam-

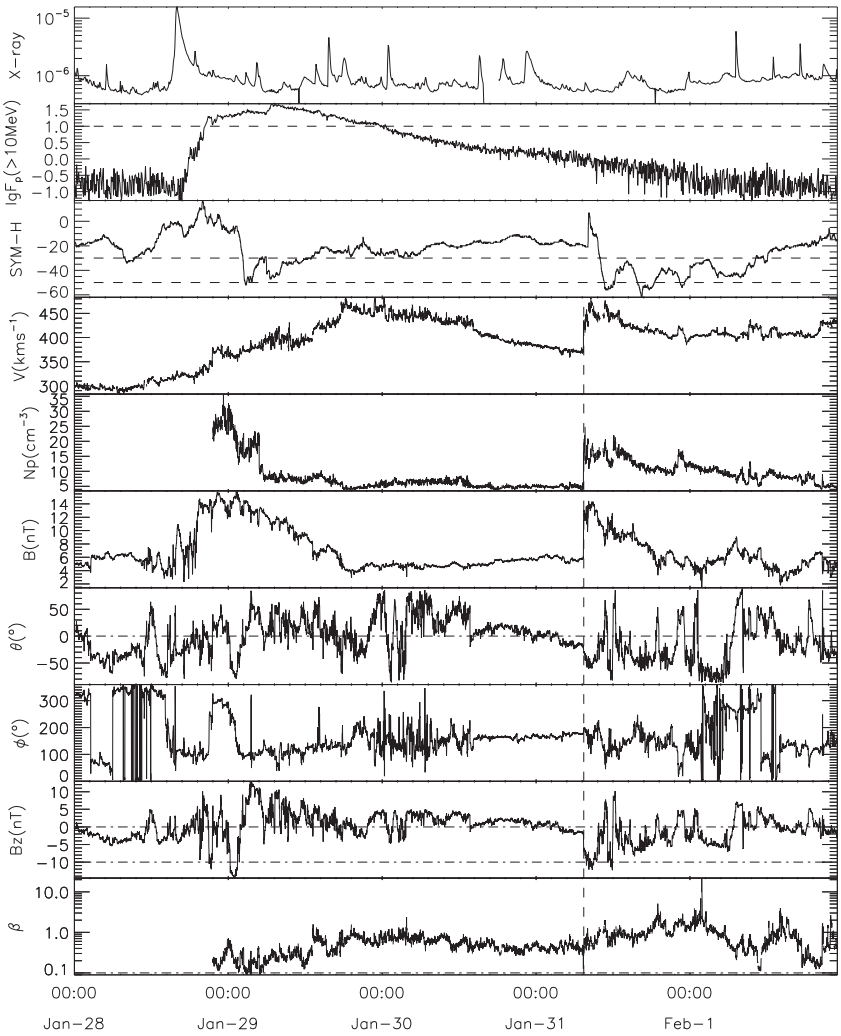

Fig. 2 The solar flare, the flux of $E > 10$ MeV protons, geomagnetic activity and the parameters of solar wind plasma during 2001 January 28 - February 1. The vertical dashed line indicates the arriving ICME-driven shock.

Table 2 Geoeffectiveness of CMEs Associated with Type-II SPEs during Solar Cycle 23

Event No.	Solar X-ray Flare					CME		>10MeV	Dst	IPS
	Date yyyy/mm/dd	Time hh:mm	Location	AR	X-ray peak	Vel. (km s^{-1})	AW (°)	Peak Flux (pfu)	(nT)	
1	1997/11/04	05:55	S14W33	8100	X2.1	785	360	72	–110	SH
2	1997/11/06	11:50	S18W63	8100	X9.4	1556	360	490	–53	SH
3	1998/05/02	13:35	S15W15	8210	X1.1	938	360	150	–205	SH
4	2000/04/04	15:41	N16W66	8933	C9.7	1188	360	55	–288	SH
5	2000/11/08	23:28	N10W75	9213	M7.4	1738	>170	14800	–96	SH
6	2001/04/15	13:50	S20W85	9415	X14	1199	167	951	–114	SH
7	2001/10/19	16:30	N15W29	9661	X1.6	901	360	11	–187	SH
8	2002/04/17	08:24	S14W34	9906	M2.6	1240	360	24	–127	SH
9	2003/10/29	20:49	S15W02	10486	X10	2029	360	1570	–383	SH
10	2003/11/02	17:15	S20W56	10486	X8.3	2598	360	353	–63	SH
11	2004/11/07	16:06	N09W17	10696	X2.0	1523	360	495	–289	SH
12	2005/01/15	23:02	N15W05	10720	X2.6	2861	360	300	–103	SH
13	2005/01/20	07:01	N14W61	10720	X7.1	882	360	1680	–97	SH
14	2005/08/22	17:27	S12W60	10798	M5.6	2738	360	330	–184	SH
15	2006/12/13	02:40	S06W23	10930	X3.4	1774	360	698	–162	MC

Notes: IPS indicates the interplanetary source of the storm, SH indicates sheath and MC indicates magnetic cloud.

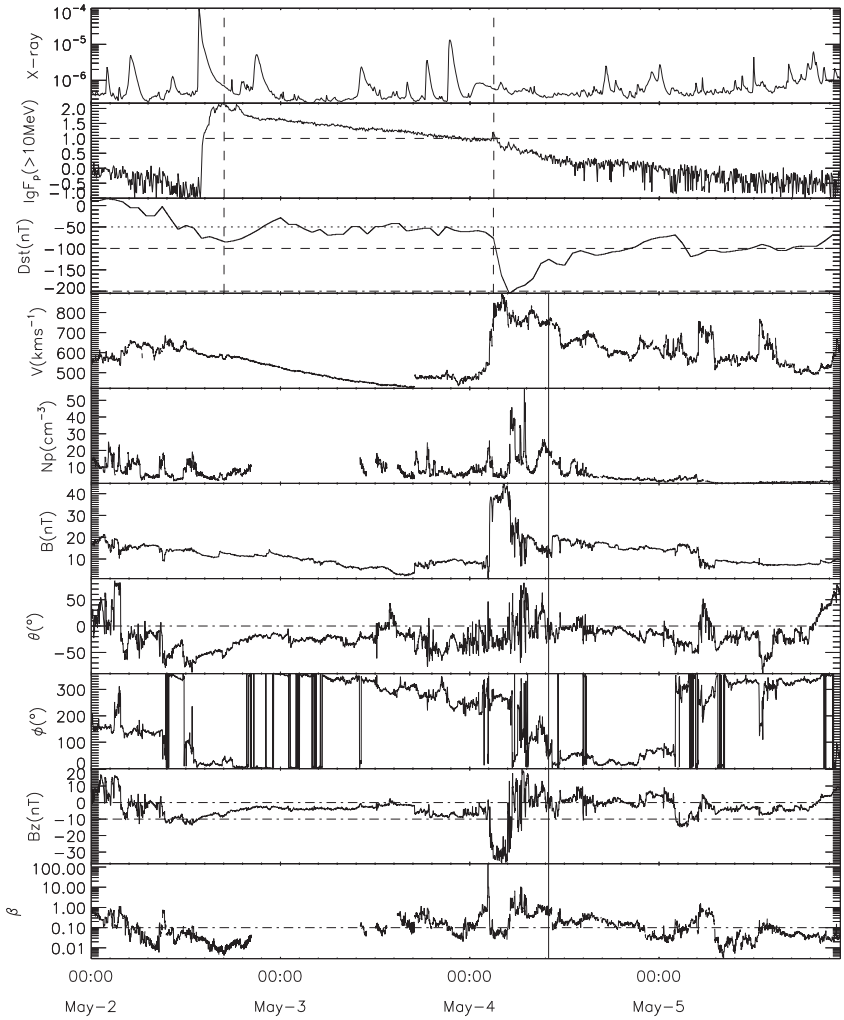

Fig. 3 The solar flare, the flux of $E > 10$ MeV protons, geomagnetic activity and the parameters of solar wind plasma during 1998 May 2 - 4. The first and second dashed vertical lines represent the first and second proton flux peak, respectively. The solid vertical line indicates the start time of the ICME.

ple that the intensity-time profile of an SPE event has two peaks and the second peak is higher than the first one.

3.3.1 Case 1

An X17.2 solar flare appeared on 2003 October 28 accompanied by a very fast full halo CME, in AR 10486 at S16E08. A relativistic solar proton (RSP) event was observed by ground-based neutron monitors. The possible acceleration mechanism of RSPs has been studied by many authors (Miroshnichenko et al. 2005; Li et al. 2007). *GOES* 10 observed a very strong SPE shown in the sixth panel from the top in Figure 5. It can be seen from Figure 5 that the SPE intensity increased quickly after the eruption of the solar flare and the CME then increased gradually in a sustained manner. The SPE intensity reached its peak value (29500 pfu) when the IP shock arrived at the magnetosphere. The vertical dashed line in Figure 5 indicates the time when the IP shock reached the magnetosphere. The solid vertical line indicates the start time of the MC. The sheath and the MC triggered a super geomagnetic storm (Dst =–353 nT). It is obvious that the main phase of the super storm was mainly caused by the MC.

3.3.2 Case 2

A long lasting M1 flare erupted at 15:14 UT, 2004 July 25, in AR 10652 (N08W33). *SOHO*/LASCO observed a full halo CME heading for the Earth. The flux of >10 MeV protons became enhanced and reached the first peak at 23:05 UT, 2004 July 25, which is indicated by the first vertical dashed line in Figure 6. The flux of >10 MeV protons reached its second peak (2090 pfu) at 22:50 UT, 2004 July 26, which is indicated by the second vertical dashed line in Figure 6. The *ACE* spacecraft not only observed the ICME-driven shock, but also observed the ICME. The vertical solid line in Figure 6 indicates the start time of the ICME. It was apparent that the geomagnetic storm associated with the SPE was an intense geomagnetic storm (Dst = –197 nT). It can be seen from Figure 6 that both

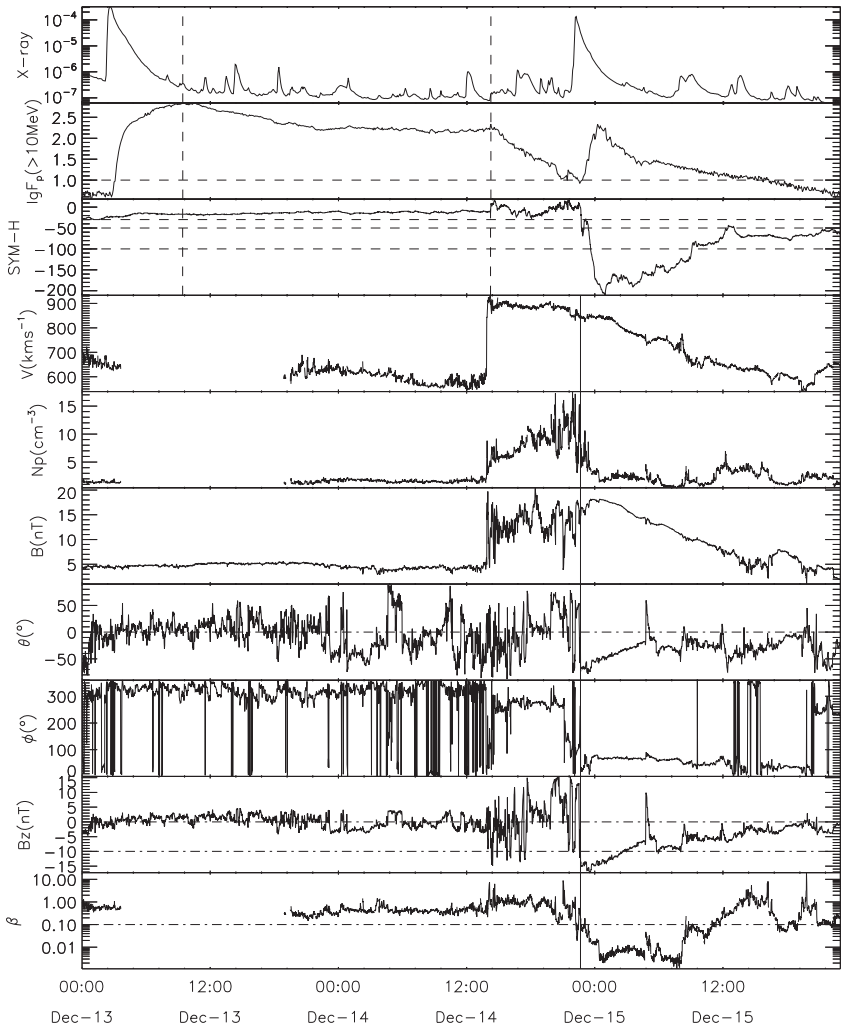

Fig. 4 The solar flare, the flux of $E > 10$ MeV protons, geomagnetic activity and the parameters of solar wind plasma during 2006 December 13 - 15. The first and second dashed vertical lines represent the first and second proton flux peak, respectively. The solid vertical line indicates the start time of the ICME.

the sheath and the ICME made a contribution to the main phase of the geomagnetic storm, however, the ICME made much more of a contribution to the main phase of the geomagnetic storm than the sheath.

3.3.3 Statistical results

Eighteen Type-III SPEs occurred during solar cycle 23. The geoeffectiveness of CMEs associated with 18 SPEs is listed in Table 3. We can see from the table that the CME associated with the SPE that began on 2002 July 15 has no geoeffectiveness. The angular width of the CME associated with the SEP event was 188°, indicating that the CME is not a halo CME. This may be the reason why the CME finally did not reach the Earth and it did not cause a geomagnetic storm. The remaining 17 SPEs listed in Table 3 were associated with full halo CMEs. All SPEs except for the one that occurred on 2002 July 15 were accompanied by geomagnetic storms. Nine geomagnetic storms were great geomagnetic storms (Dst$\leq$ –200 nT). The solar wind structure that played a key role in producing the geomagnetic storm is expressed by the underlined bold text in the last column of Table 3. We can see from the table that a considerable number of geomagnetic storms associated with SPEs having a Type-III profile were mainly produced either by the associated ICME or by an MC, suggesting that the corresponding CMEs headed for the Earth and finally passed the Earth.

4 DISCUSSION

The ICMEs associated with SPEs with a Type-I profile always missed the magnetosphere. The ICME-driven shocks did not reach the magnetosphere in most cases. Since ICMEs are very large in scale, if only the shock passes the *ACE* spacecraft but the ICME misses it, the location of *ACE* must be near the far flank of the ICME where the shock is not strong. Consequently, the solar wind compression across the shock would not generate a strong southward turbulent magnetic field, which explains the fact that

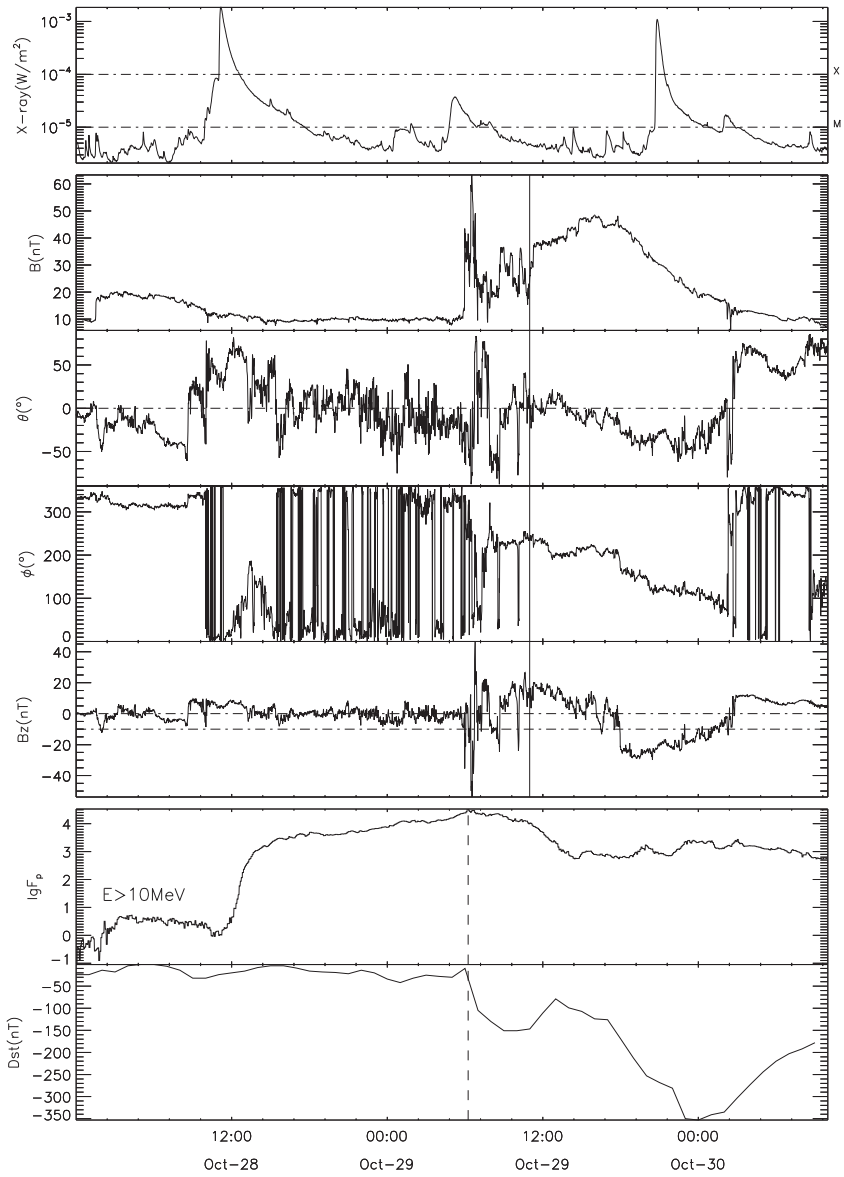

Fig. 5 The solar flare, the flux of $E > 10$ MeV protons, geomagnetic activity and the parameters of solar wind plasma during 2003 October 28–30. The dashed vertical line indicates the arriving IP shock and the peak proton flux. The solid vertical line indicates the start time of the ICME.

such kinds of SPEs are usually not associated with intense geomagnetic storms. It can be seen from Table 1 that the majority of Type-I events are not associated with geomagnetic storms, with only a few having small or moderate storms, but never an intense one.

After the rapid rise to the first peak, the intensity of SPEs with Type-II profiles decreased very slowly and then reached its second peak, implying that the SEPs observed by *GOES* were accelerated by the shock not far from the shock nose. The distance between the location, where particles were accelerated, and the shock nose gradually increases as the ICME and its driven shock move away from the Sun. When an ICME-driven shock reaches the magnetosphere, the SPE reaches its second peak, implying that the shock is still strong and the location, where particles were accelerated and observed by *GOES*, is still not too far away from the nose of the shock when reaching the magnetosphere. This may be the reason why both the shock sheath and ICME associated with the SPEs having a Type-II profile can finally reach the magnetosphere and cause a geomagnetic storm. However, most of the storms were only caused by the sheath. This suggests that in most cases the ICMEs associated with Type-II SPEs move towards the Earth when the ICMEs propagate in IP space, however, maybe only the shocks and the ICME flanks pass the Earth.

The outstanding property of the SPEs with a Type-III profile is the sustained enhancement of particle intensity, or the second peak is higher than the first one in magnitude. The sustained enhancement of particle intensity indicates that particles are accelerated by the shock near the nose,

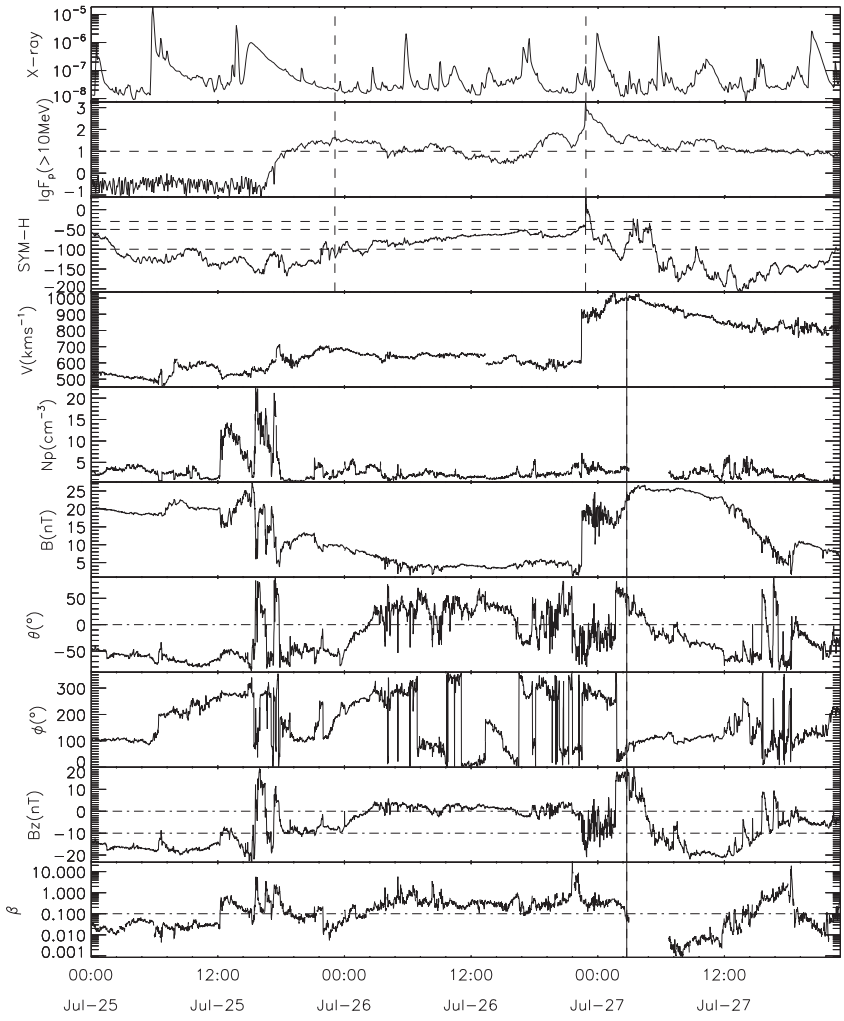

Fig. 6 The solar flare, the flux of $E > 10$ MeV protons, geomagnetic activity and the parameters of solar wind plasma during 2004 July 25–27. The first and second dashed vertical lines represent the first and second proton flux peak, respectively. The solid vertical line indicates the start time of the ICME.

and the acceleration can be sustained until the shock passes the Earth. Consequently, both the shock and the ICME can pass a spacecraft located at the L1 point. The main phases of geomagnetic storms associated with the Type-III events were mainly caused by the ICMEs or MCs (Table 3), implying that the ICME core may pass the Earth. The SPE that occurred on 2005 September 7 is an exception because the ICME associated with the SPE was not observed by *ACE*. The source location of the CME is S06E77, far away from the solar disk center, and this may be the reason why only the CME-driven shock passed the *ACE* spacecraft. In most cases, both the ICME and the ICME-driven shock associated with the SPEs having a Type-III profile move towards the Earth and finally pass the Earth and then produce a very strong storm.

The solar source of an intense geomagnetic storm is either a CME or a coronal hole, or the combination of them. According to the final Dst index data (*http://wdc.kugi.kyoto-u.ac.jp/dst_final/index.html*) and the investigation of solar and interplanetary sources for each intense geomagnetic storm that occurred during solar cycle 23 (Le et al. 2012, 2013; Zhang et al. 2007; Echer et al. 2008), the number of intense geomagnetic storms (–200 nT$<$Dst$\leq$ –100 nT) associated with CMEs during solar cycle 23 is 58. The result of the present paper shows that only a small part (13/58) of intense geomagnetic storms were associated with SPEs. Seventeen great geomagnetic storms (Dst$\leq$ –200 nT) were registered during solar cycle 23 and 13 of them were accompanied by Type-II or Type-III SPEs.

For the Type-II SPEs, the lead-time is defined as the time interval from the time when the flux began to increase before the occurrence of the second peak of the SPE to the the start time of the main phase of the associated geomagnetic storm. The lead-time has been checked for each SPE listed in Table 2. The results show that lead-time ranged from tens of minutes to more than 10 h. The average lead-time is about 5 h.

For Type-III SPEs, the lead-time is defined the same as Type-II SPEs if the profile of the SPE has two peaks. If the

Table 3 Geoeffectiveness of CMEs Associated with Type-III SPEs during Solar Cycle 23

Event	Solar X-ray flare					CME		>10 MeV	Dst	IPS
No.	Date yyyy/mm/dd	Time hh:mm	Location	AR	X-ray peak	Vel. (km s^{-1})	AW (°)	Peak flux (pfu)	(nT)	
1	1998/08/24	22:05	N30E07	8307	X1	DG	DG	670	–155	SH+**ICME**
2	1998/09/23	07:00	N18E09	8340	M7	DG	DG	44	–207	MC
3	2000/06/06	15:25	N20E18	9026	X2.3	1119	360	84	–90	SH
4	2000/07/14	10:24	N22W07	9077	X5.7	1674	360	24000	–301	MC
5	2000/08/09	15:25	N11W11	9114	C2.3	702	360	17	–235	SH+**MC**
6	2001/03/29	10:15	N14W12	9402	X1.7	942	360	35	–387	SH+**MC**
7	2001/04/10	05:26	S23W09	9415	X2.3	2411	360	355	–271	**SH**+MC
8	2001/09/24	10:38	S16E23	9632	X2.6	2402	360	12900	–102	SH
9	2001/11/04	16:20	N06W18	9684	X1.0	1810	360	31700	–292	MC + **PMC-SH**+ICME
10	2001/11/22	23:30	S15W34	9704	M9.9	1437	360	18900	–221	**SH** + ICME
11	2002/05/22	03:54	S19W56	ND	C5.0	1557	360	820	–109	SH
12	2002/07/15	20:08	N19W01	10030	M1.8	1151	188	234	0	
13	2002/09/05	17:06	N09E28	10102	C5.2	1748	360	208	–181	**PICME-SH** + ICME
14	2003/05/28	00:27	S07W17	10365	X3.6	1366	360	121	–144	SH
15	2003/10/28	11:10	S16E08	10486	X17	2459	360	29500	–353	SH+**MC**
16	2004/07/25	15:14	N08W33	10652	M1.1	1333	360	2086	–170	SH+**MC**
17	2005/05/13	16:57	N12E11	10759	M8.0	1689	360	3140	–247	SH+**MC**
18	2005/09/07	17:40	S06E77	10808	X17.0	NA	NA	1800	–147	SH

Notes: DG indicates a data gap, ND indicates no data.

flux of SPEs increased impulsively at the early phase and then increased gradually in a sustained manner, then the lead-time is defined as the time interval from the time when SPE intensity began to gradually increase to the start time of the main phase of the associated geomagnetic storm. The lead-time for the SPEs listed in Table 3 ranged from several hours to more than 20 h. The average lead-time was about 18 h.

If an IP shock is approaching the Earth, the flux of SEPs observed by *GOES* may be enhanced. This suggests that the intensity-time profile of SEP events can provide dynamic information about the ICMEs and the propagation of shocks driven by ICMEs in the IP medium, which can be used to predict the geoeffectiveness of the CMEs associated with SEP events. The results of this paper suggest that only a small part of the intense geomagnetic storms can be predicted by the information implied in the intensity-time profile of SPEs. However, most of the great geomagnetic storms can be predicted by the information implied in the intensity-time profile of SPEs. If we use the intensity-time profile of protons with energy lower than 10 MeV, more intense and great geomagnetic storms can be predicted. This is the goal of our work in the near future.

5 SUMMARY AND CONCLUSIONS

The geoeffectiveness of CMEs accompanied by SPEs with three intensity-time profiles has been investigated. The analysis has led to the following conclusions:

(1) The CMEs associated with Type-I SPEs always missed the Earth and only a small part of the CME-driven shock passed the Earth. Most of the CMEs associated with Type-I SPEs had no geoeffectiveness. Only a small part of CMEs associated with Type-I SPEs produced small or moderate geomagnetic storms, but never an intense one.

(2) Both the CMEs and CME-driven shocks associated with Type-II SPEs could pass the Earth. Most CMEs associated with Type-II SPEs produced intense or great geomagnetic storms. Only a small part of CMEs associated with Type-II SPEs produced moderate geomagnetic storms. In most cases, the IP sources responsible for the main phases of the storms were the shock sheaths.

(3) Both the CME and CME-driven shock associated with Type-III SPEs could reach the Earth. A considerable part of the CMEs associated with Type-III SPEs produced great geomagnetic storm at the level of Dst$\leq$ –200 nT. Others would produce intense geomagnetic storms. A considerable part of the geomagnetic storms associated with Type-III SPEs were mainly caused by MCs or ICMEs.

(4) Only a small part of the intense geomagnetic storms were associated with SPEs. However, most of the great geomagnetic storms were associated with SPEs.

Acknowledgements We thank NOAA for providing the solar soft X-ray and SPE data, and the Data Analysis Center for Geomagnetism and Space Magnetism, Kyoto University, for providing the Dst and SYM-H indexes. We would like to thank the *ACE* SWEPAM instrument team and the *ACE* Science Center for providing *ACE* data. This work is supported by the National Basic Research Program of China (973 Program, Grant No. 2012CB957801), the National Natural Science Foundation of China (Grant Nos. 41074132, 41274193, 41674166, 41031064 and 11303017) and the National Standard Research Program (Grant No. 200710123). C. Li would like to thank the project 985 of Nanjing University, the Advanced

Discipline Construction Project of Jiangsu Province and the NKBRSF (Grant No. 2014CB744203).

References

Bisi, M. M., Breen, A. R., Jackson, B. V., et al. 2010, Sol. Phys., 265, 49
Brueckner, G. E., Howard, R. A., Koomen, M. J., et al. 1995, Sol. Phys., 162, 357
Cane, H. V., Reames, D. V., & von Rosenvinge, T. T. 1988, J. Geophys. Res., 93, 9555
Cane, H. V., von Rosenvinge, T. T., Cohen, C. M. S., & Mewaldt, R. A. 2003, Geophys. Res. Lett., 30, 8017
Cane, H. V., Mewaldt, R. A., Cohen, C. M. S., & von Rosenvinge, T. T. 2006, Journal of Geophysical Research (Space Physics), 111, 6
Echer, E., Gonzalez, W. D., Tsurutani, B. T., & Gonzalez, A. L. C. 2008, Journal of Geophysical Research (Space Physics), 113, 5221
Gopalswamy, N., Yashiro, S., Michałek, G., et al. 2002, ApJ, 572, L103
Gopalswamy, N., Yashiro, S., Krucker, S., Stenborg, G., & Howard, R. A. 2004, Journal of Geophysical Research (Space Physics), 109, 12105
Gopalswamy, N., Yashiro, S., & Akiyama, S. 2007, Journal of Geophysical Research (Space Physics), 112, 6112
Hutchinson, J. A., Wright, D. M., & Milan, S. E. 2011, Journal of Geophysical Research (Space Physics), 116, 9211
Kahler, S. W. 2001, J. Geophys. Res., 106, 20947
Kahler, S. W. 2005, ApJ, 628, 1014
Kahler, S. W., & Vourlidas, A. 2005, Journal of Geophysical Research (Space Physics), 110, 12
Kallenrode, M.-B. 2003, Journal of Physics G Nuclear Physics, 29, 965
Kim, R.-S., Cho, K.-S., Kim, K.-H., et al. 2008, ApJ, 677, 1378
Kim, R.-S., Cho, K.-S., Moon, Y.-J., et al. 2010, Journal of Geophysical Research (Space Physics), 115, 12108
Le, G.-M., Tang, Y.-H., & Han, Y.-B. 2006, ChJAA (Chin. J. Astron. Astrophys.), 6, 751
Le, G., Cai, Z., Wang, H., & Zhu, Y. 2012, Astrophys. Space Sci. 339, 151
Le, G.-M., Cai, Z.-Y., Wang, H.-N., Yin, Z.-Q., & Li, P. 2013, RAA (Research in Astronomy and Astrophysics), 13, 739
Le, G., Yang, X., Ding, L., et al. 2014, Ap&SS, 352, 403
Li, C., Tang, Y. H., Dai, Y., Fang, C., & Vial, J.-C. 2007, A&A, 472, 283
Li, G., & Zank, G. P. 2005, Geophys. Res. Lett., 32, 2101
Liu, Y., Davies, J. A., Luhmann, J. G., et al. 2010a, ApJ, 710, L82
Liu, Y., Thernisien, A., Luhmann, J. G., et al. 2010b, ApJ, 722, 1762
Miroshnichenko, L. I., ed. 2001, Astrophysics and Space Science Library, 260, Solar Cosmic Rays (Kluwer Academic Publishers)
Miroshnichenko, L. I., Klein, K.-L., Trottet, G., et al. 2005, Journal of Geophysical Research (Space Physics), 110, 9
Miroshnichenko, L. I., & Perez-Peraza, J. A. 2008, International Journal of Modern Physics A, 23, 1
Moon, Y.-J., Cho, K.-S., Dryer, M., et al. 2005, ApJ, 624, 414
Pérez-Peraza, J., Vashenyuk, E. V., Miroshnichenko, L. I., Balabin, Y. V., & Gallegos-Cruz, A. 2009, ApJ, 695, 865
Qin, G., Zhang, M., & Dwyer, J. R. 2006, Journal of Geophysical Research (Space Physics), 111, 8101
Qin, G., Wang, Y., Zhang, M., & Dalla, S. 2013, ApJ, 766, 74
Reames, D. V. 1999, Space Sci. Rev., 90, 413
Richardson, I. G., & Cane, H. V. 2010, Sol. Phys., 264, 189
Simnett, G. M. 2006, A&A, 445, 715
Smith, Z., Murtagh, W., & Smithtro, C. 2004, Journal of Geophysical Research (Space Physics), 109, 1110
Smith, Z. K., & Murtagh, W. J. 2009, Advances in Space Research, 44, 775
Takeuchi, T., Russell, C. T., & Araki, T. 2002, Journal of Geophysical Research (Space Physics), 107, 1423
Trottet, G., Samwel, S., Klein, K.-L., Dudok de Wit, T., & Miteva, R. 2015, Sol. Phys., 290, 819
Tsurutani, B. T., Gonzalez, W. D., Gonzalez, A. L. C., et al. 1995, J. Geophys. Res., 100, 21717
Tylka, A. J., Cohen, C. M. S., Dietrich, W. F., et al. 2005, ApJ, 625, 474
Valtonen, E., Laitinen, T., & Huttunen-Heikinmaa, K. 2005, Advances in Space Research, 36, 2295
Wanliss, J. A., & Showalter, K. M. 2006, Journal of Geophysical Research (Space Physics), 111, 2202
Wilken, B., Goertz, C. K., Baker, D. N., Higbie, P. R., & Fritz, T. A. 1982, J. Geophys. Res., 87, 5901
Zank, G. P., Li, G., & Verkhoglyadova, O. 2007, Space Sci. Rev., 130, 255
Zhang, J., Richardson, I. G., Webb, D. F., et al. 2007, Journal of Geophysical Research (Space Physics), 112, 10102